Supporting Information

Biomimetic nanoclay hydrogel with cascade catalytic and photothermal functions for wound therapy

Qianqian Liu[a], Weimin Xie[a], Juan Liao[a], Yuhan Ma[a,b], Xiaozheng Liang[a], Yili Tang[a], Hao Wang[a,b,c], Huaming Yang[a, b,c]*

[a] Engineering Research Center of Nano-Geomaterials of Ministry of Education, China University of Geosciences, Wuhan 4c0074, China, E-mail: hm.yang@cug.edu.cn (H. Yang)

[b] Faculty of Materials Science and Chemistry, China University of Geosciences, Wuhan 4c0074, China

[c] Laboratory of Advanced Mineral Materials, China University of Geosciences, Wuhan 4c0074, China

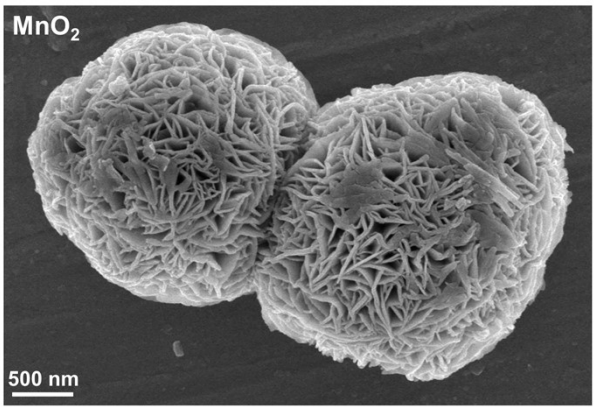

Figure S1. SEM image of MnO_2.

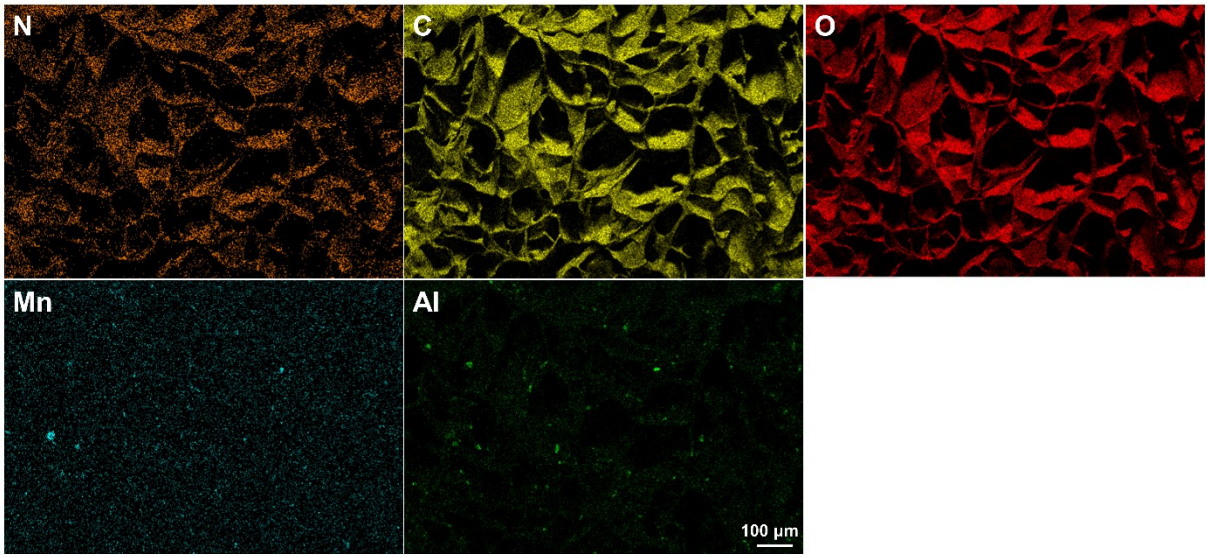

Figure S2 Elemental mapping of N, C, O, Mn and Al in the MnO_2@MMT/CS hydrogel.

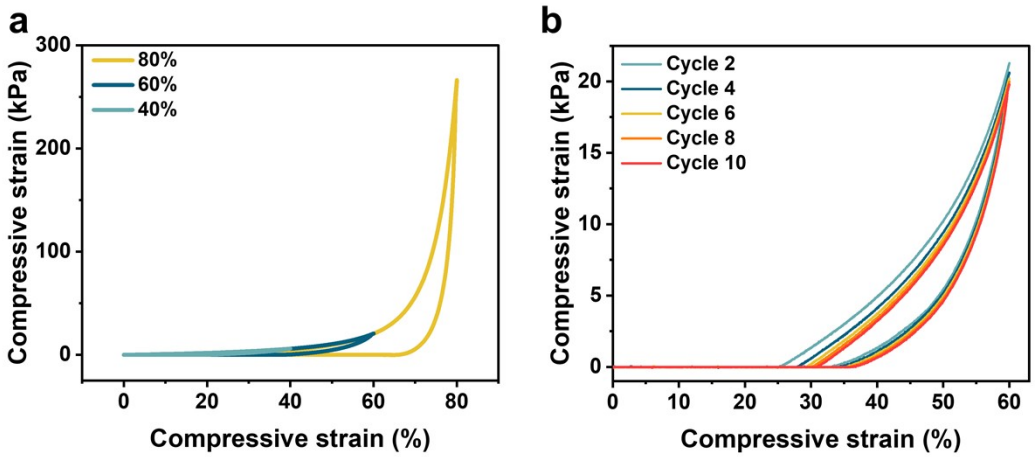

Figure S3 Cyclic compressive behavior and strain-dependent mechanical performance of the MnO_2@MMT/CS hydrogel. (a) Compressive stress–strain curves at increasing strain levels. (a) Stress–strain responses under repeated compression cycles at 60% compressive strain.

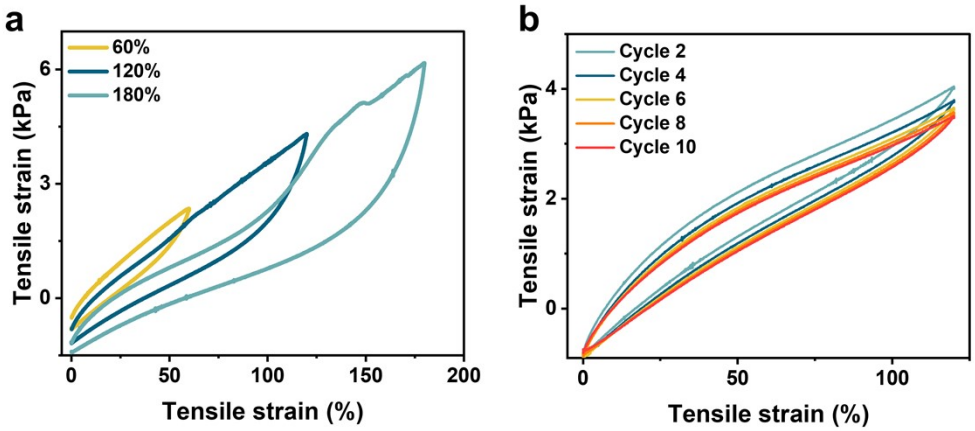

Figure S4 Tensile mechanical behavior and cyclic tensile performance of the MnO_2@MMT/CS hydrogel. (a) Tensile stress–strain curves at increasing tensile strain levels. (b) Stress–strain responses under repeated tensile cycles at 120% tensile strain.

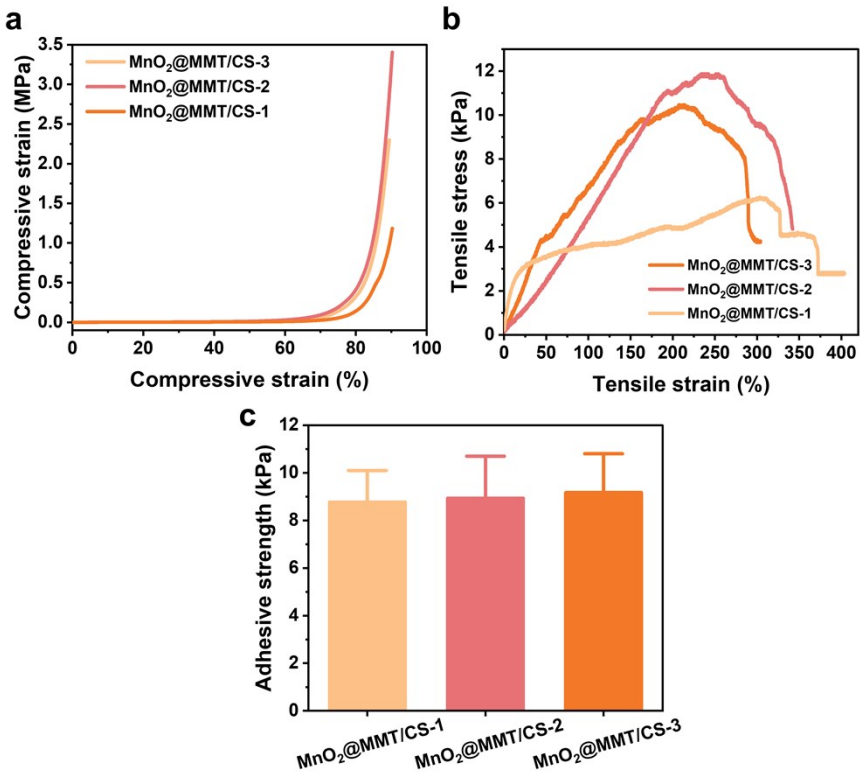

Figure S5 Mechanical and adhesive properties of MnO_2@MMT/CS hydrogels with different composite ratios. (a) Compressive stress–strain curves of the hydrogels. (b) Tensile stress–strain curves of the hydrogels. (c) Adhesive strength of the hydrogels on biological tissue. Data are presented as mean ± SD (n = 3). MnO_2@MMT/CS-1, MnO_2@MMT/CS-2, and MnO_2@MMT/CS-3 represent MnO_2@MMT loading amounts of 50 mg, 250 mg, and 1250 mg, respectively.

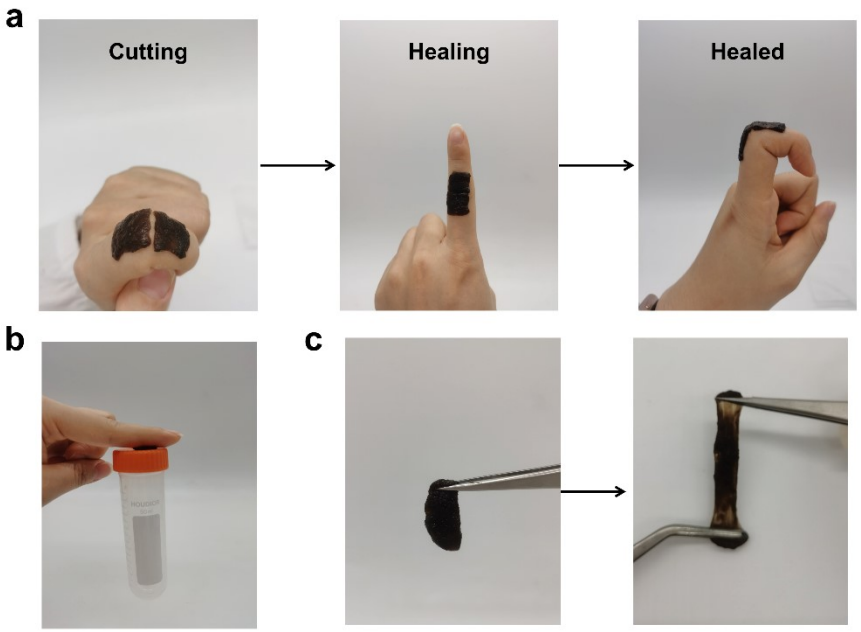

Figure S6. Macroscopic demonstrations of the mechanical and adhesive properties of the MnO_2@MMT/CS hydrogel. (a) Self-healing capability. (b) Tissue adhesion property. (c) Extensibility.

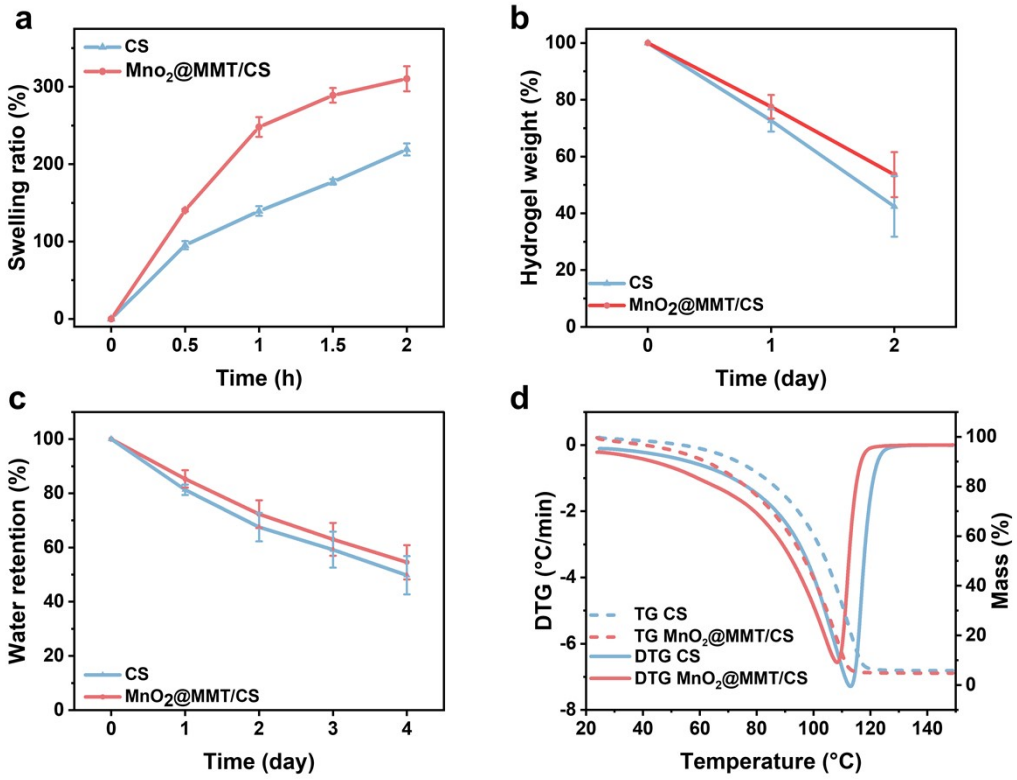

Figure S7. Swelling, degradation, and water retention properties of CS and MnO_2@MMT/CS hydrogels. (a) Swelling ratio of the hydrogels as a function of immersion time. (b) In vitro degradation behavior of the hydrogels. (c) Water retention behavior of the hydrogels over time at 37 ℃. (d) TG analysis curve and DTG c curve of hydrogels.

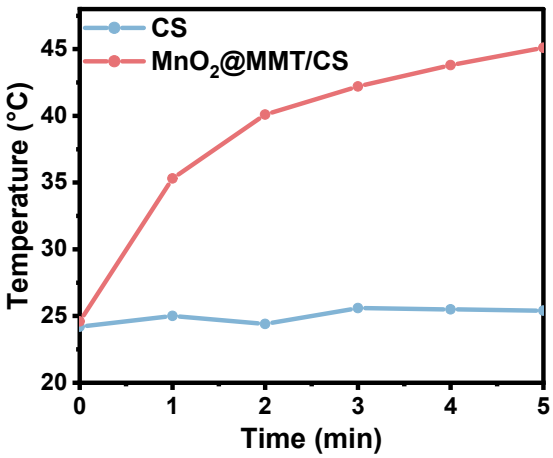

Figure S8 Temperature variation curve of the MnO_2@MMT/CS hydrogel under 808 nm laser irradiation (1 W/cm^2).

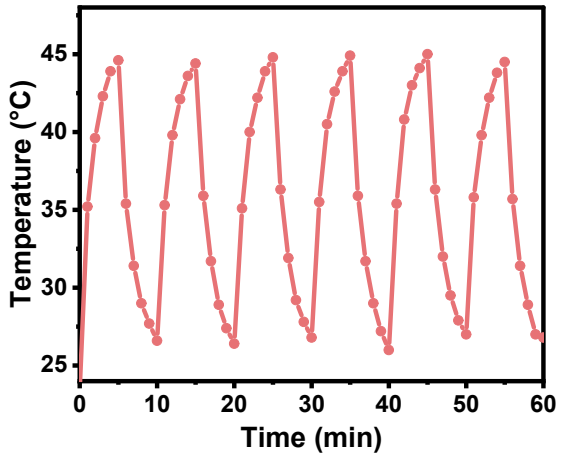

Figure S9. Cyclic photothermal heating curves of the MnO_2@MMT/CS hydrogel over five cycles (5 min light ON / 5 min light OFF per cycle).

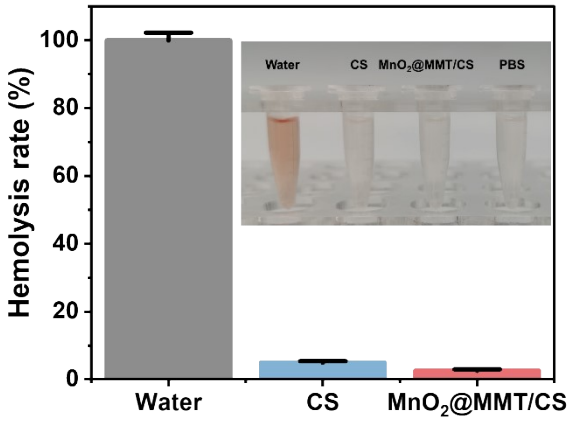

Figure S10. Hemolytic properties of different materials. Data are presented as mean ± SD (n = 3).

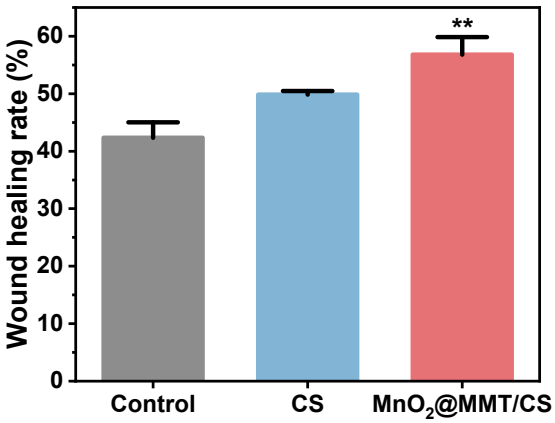

Figure S11. Comparison of HaCaT cell migration among different treatment groups. Data are presented as mean ± SD (n = 3). Statistical analysis was performed using one-way ANOVA followed by Tukey's post hoc test, with comparisons conducted between each treatment group and the control group. *$p \leq 0.05$, ** $p \leq 0.01$, *** $p \leq 0.001$.

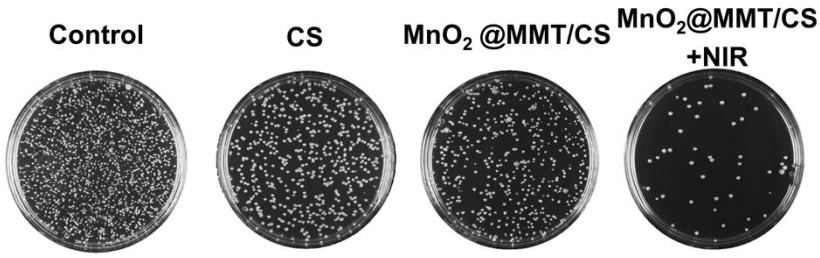

Figure S12. Bacterial colony images on wounds from different treatment groups.

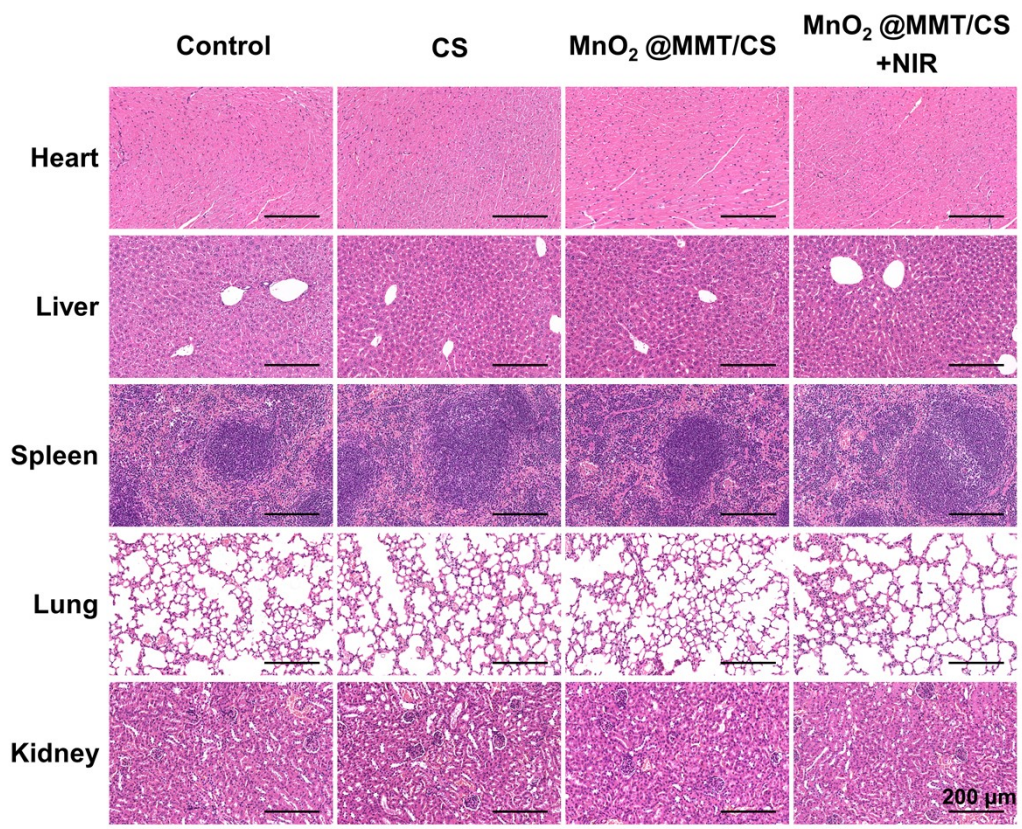

Figure S13. Histological analysis of hearts, livers, spleens, lungs, and kidneys in different treatment groups by H&E staining.